Isoparametric Graded Finite Elements for Nonhomogeneous Isotropic and Orthotropic Materials

Jeong-Ho Kim

G. H. Paulino[1]
Mem. ASME,
e-mail: paulino@uiuc.edu

Department of Civil and Environmental Engineering,
University of Illinois at Urbana-Champaign,
Newmark Laboratory,
205 North Mathews Avenue,
Urbana, IL 61801

Graded finite elements are presented within the framework of a generalized isoparametric formulation. Such elements possess a spatially varying material property field, e.g. Young's modulus (E) and Poisson's ratio (ν) for isotropic materials; and principal Young's moduli (E_{11},E_{22}), in-plane shear modulus (G_{12}), and Poisson's ratio (ν_{12}) for orthotropic materials. To investigate the influence of material property variation, both exponentially and linearly graded materials are considered and compared. Several boundary value problems involving continuously nonhomogeneous isotropic and orthotropic materials are solved, and the performance of graded elements is compared to that of conventional homogeneous elements with reference to analytical solutions. Such solutions are obtained for an orthotropic plate of infinite length and finite width subjected to various loading conditions. The corresponding solutions for an isotropic plate are obtained from those for the orthotropic plate. In general, graded finite elements provide more accurate local stress than conventional homogeneous elements, however, such may not be the case for four-node quadrilateral (Q4) elements. The framework described here can serve as the basis for further investigations such as thermal and dynamic problems in functionally graded materials. [DOI: 10.1115/1.1467094]

1 Introduction

Recent advances in material processing have allowed manufacturing a wide diversity of functionally graded materials (FGMs) ([1–3]). Such materials possess continuously graded properties with gradual change in microstructure ([4,5]). The materials are made to take advantage of desirable features of its constituent phases. For instance, in a thermal protection system, FGMs take advantage of heat and corrosion resistance typical of ceramics, and mechanical strength and toughness typical of metals.

FGMs are nonhomogeneous with regard to thermomechanical and strength related properties. Depending on the processing technique, they may exhibit either isotropic or anisotropic material properties. For instance, large bulk FGMs produced by spark plasma sintering (SPS) technique may be modeled as isotropic materials ([6]). On the other hand, materials processed using plasma spray technique have generally a lamellar structure ([7]), while materials processed by electron beam physical vapor deposition (PVD) may have a columnar structure ([8]). Thus, in studying the mechanics of the former class of materials (fabricated by SPS), a nonhomogeneous isotropic model may be appropriate; and for the latter class of materials (fabricated by plasma spraying or PVD), a nonhomogeneous orthotropic model may suffice as a first approximation. Thus, both types of material models, i.e., isotropic and orthotropic, are investigated here.

As the manufacturing of FGMs advances, new modeling techniques are also developed for such materials ([3,9]). Here, we focus on the finite element method for nonhomogeneous materials using a generalized isoparametric formulation. The graded elements obtained with this formulation are compared with conventional homogeneous elements, as illustrated by Fig. 1. Notice that the graded element incorporates the material property gradient at the size scale of the element, while the homogeneous element produces a stepwise constant approximation to a continuous material property field such as the one shown in Fig. 1.

This paper discusses and compares the behavior of graded versus conventional homogeneous elements under various loading conditions in both isotropic and orthotropic FGMs with respect to analytical solutions which are either available in the literature or derived in this work. The manuscript is organized as follows. The next subsection presents an example which serves as a motivation to this work. In this example, the FGM leads to a stress redistribution with lower stress concentration factor (SCF) than the corresponding problem with homogeneous material. Next, a brief literature survey and comments on previous related work are given. Section 2 presents some exact solutions for displacements and stresses in orthotropic FGMs. The exact solutions for isotropic FGMs are obtained as particular instances of those for orthotropic FGMs. Section 3 reviews finite element formulations. Section 4 addresses the generalized isoparametric graded finite element formulation. Sections 5 and 6 present finite element results for stresses in isotropic and orthotropic FGMs, respectively, which are compared with analytical solutions. Finally, Section 7 provides some concluding remarks.

1.1 Motivation. Functionally graded composites, with smooth variation of volume fractions, offer various advantages such as reduction of residual stress ([10]) and increased bonding strength ([11]). Moreover, if properly used, such materials may also lead to reduction of stress concentration or stress intensity factors ([12]). For example, Hasselman and Youngblood ([13]) found that the maximum tensile thermal stresses in brittle ceramics can be reduced significantly by spatially varying thermal conductivity in a hollow circular cylinder subjected to radially inward or outward steady-state heat flow, and Horgan and Chan ([14]) investigated the effect of material nonhomogeneity on the response of linearly elastic isotropic hollow circular cylinders or

[1]To whom correspondence should be addressed.

Contributed by the Applied Mechanics Division of THE AMERICAN SOCIETY OF MECHANICAL ENGINEERS for publication in the JOURNAL OF APPLIED MECHANICS. Manuscript received by the ASME Applied Mechanics Division, July 2, 2001; final revision Nov. 14, 2001. Associate Editor: M.-J. Pindera. Discussion on the paper should be addressed to the Editor, Professor Lewis T. Wheeler, Department of Mechanical Engineering, University of Houston, Houston, TX 77204-4792, and will be accepted until four months after final publication of the paper itself in the THE AMERICAN SOCIETY OF MECHANICAL ENGINEERS JOURNAL OF APPLIED MECHANICS.

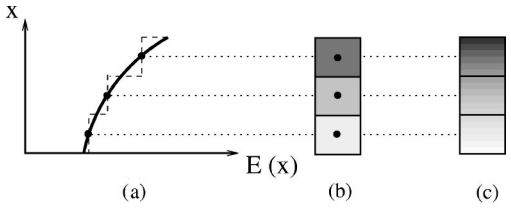

Fig. 1 Homogeneous versus graded finite elements. (*a*) Property variation along one coordinate axis; (*b*) homogeneous elements; (*c*) graded elements. Notice that the property of the homogeneous element corresponds to the property at the centroid of the graded element.

disks under uniform internal or external pressure by varying Young's modulus with respect to the radial direction and found that the maximum hoop stress in a nonhomogeneous material does not, in general, occur on the inner surface in contrast with a homogeneous material.

To further motivate the use of FGMs in engineering applications, consider the isotropic FGM link bar of Fig. 2(*a*). The bar has unit thickness, it is subjected to unit axial tension load at the right end, and it is considered in a state of generalized plane stress. The basic FGM constituents are titanium monoboride (TiB) and commercially pure titanium (CP Ti) as illustrated by Fig. 2(*b*). The elastic properties of the base materials are ([15])

$$E_{TiB}=375\ \text{GPa}, \quad \nu_{TiB}=0.14$$

$$E_{Ti}=107\ \text{GPa}, \quad \nu_{Ti}=0.34.$$

The graded region is incorporated with an exponential material variation. Thus Young's modulus and Poisson's ratio are functions of the Cartesian coordinate y (see Fig. 2), i.e.,

$$E(y)=E_{Ti}e^{\beta_E y}, \quad \nu(y)=\nu_{Ti}e^{\beta_\nu y}, \tag{1}$$

respectively, where $1/\beta_E$ and $1/\beta_\nu$ are the length scales of nonhomogeneity which are given by

$$\beta_E=\frac{1}{W}\log(E_{TiB}/E_{Ti}), \quad \beta_\nu=\frac{1}{W}\log(\nu_{TiB}/\nu_{Ti}), \tag{2}$$

respectively, where W is the width of the symmetric model as shown in Fig. 2(*b*). Figure 3(*a*) shows the finite element mesh for the symmetric portion of the link bar with 1000 quadrilateral elements of eight nodes (Q8). These elements are graded finite elements as illustrated by Fig. 1 and explained subsequently in this paper. Figure 3(*b*) shows the σ_{xx} stress contour for the homogeneous link bar (either TiB or Ti) and Fig. 3(*c*) shows the σ_{xx} stress contour for the FGM link bar (TiB/Ti). The main stress values (nodal average) are summarized in Table 1. Notice that the maximum stress location in the FGM bar is different from that in the homogeneous bar—the maximum stress occurs in A' (see Fig. 2(*b*)) for the homogeneous bar, while it occurs in B' (see Fig. 2(*b*)) for the FGM bar. Moreover, the maximum stress is lower in the FGM than in the homogeneous bar. Thus, the FGM leads to stress redistribution with a lower SCF as illustrated by Table 1 and Fig. 3. In summary, this example shows, by means of elastic finite element analysis, that *the stress response of (inhomogeneous) FGMs differ substantially from those of their homogeneous counterparts*.

1.2 Related Numerical Work. Several numerical models have been used to investigate FGMs, including integral equations (e.g., [16–18]), the higher order model (e.g., [19,20]), boundary elements (e.g., [21,22]), and finite elements (e.g., [10,23–30]). This work concentrates on the finite element method for FGMs using the isoparametric concept for graded elements.

A few additional comments about the related work by Santare and Lambros ([30]) are in order. They have also published in this journal a graded finite element model for nonhomogeneous materials. However, their work differs from ours in the sense that they sample the material properties directly at the Gauss points of the element, while we adopt a generalized isoparametric formulation. Although the two methods are different, they are equivalent for fine mesh discretizations ([31]). They investigated the behavior of

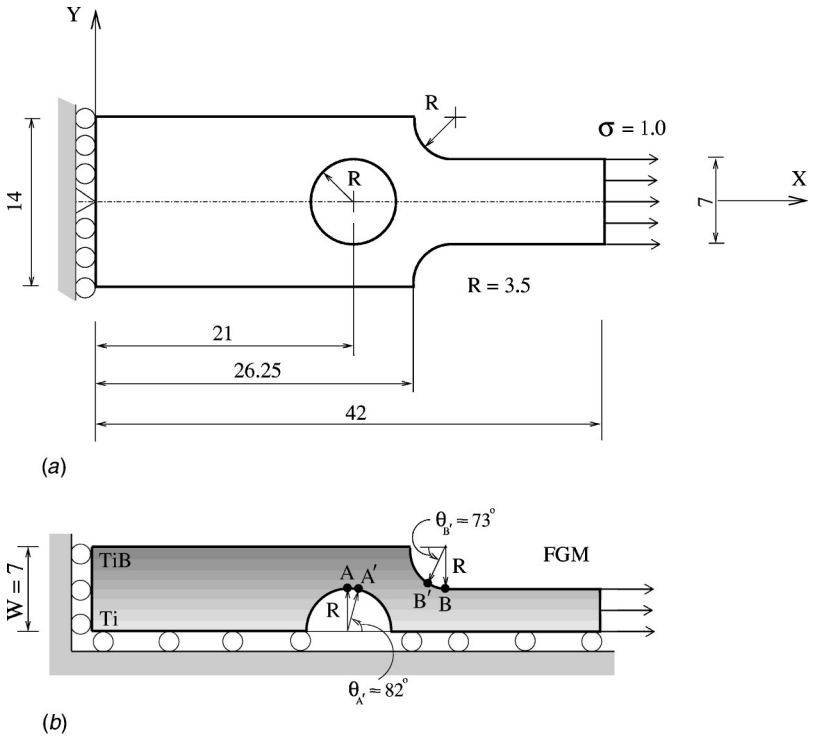

Fig. 2 FGM link bar (units: N, mm): (*a*) geometry and boundary conditions; (*b*) symmetric model

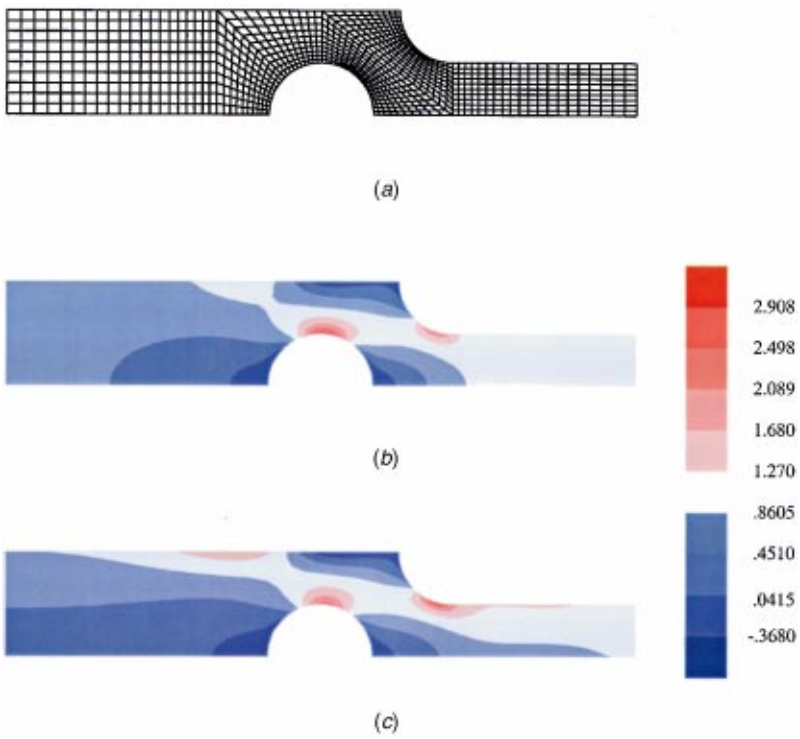

Fig. 3 FGM link bar under unit axial tension (units: N/mm^2): (*a*) mesh configuration with 1000 graded Q8 elements; (*b*) σ_{xx} stress distributions for homogeneous link bar (both TiB and Ti); (*c*) σ_{xx} stress distributions for FGM bar (TiB/Ti)

Table 1 Representative σ_{xx} stress values (N/mm^2) for the link bar of Figs. 2 and 3

	Location	
σ_{xx}	A'	B'
Homogeneous	2.908	2.137
FGM	2.369	2.601

four-node quadrilaterals (Q4) for isotropic FGMs only. In addition to the bilinear element (Q4), we also investigate the behavior of eight-node quadrilaterals (Q8) for both isotropic and orthotropic FGMs. They investigated exponential material variation only. Here, we compare both exponential and linear material variations. Finally, we believe that the generalized isoparametric formulation is more natural to the finite element method than the Gauss point sampling of material properties because the generalized formulation embraces the important isoparametric concept—the same shape functions are used to interpolate the unknown displacements, the geometry, and the material parameters.

2 Some Exact Solutions for Nonhomogeneous Elasticity

Exact solutions for both isotropic and orthotropic functionally graded materials (FGMs) will be used as reference solutions for the numerical examples that follow. We consider an *orthotropic* functionally graded plate of infinite length and finite width subjected to various loading conditions such as remote fixed grip, tension, and bending, as shown in Fig. 4. Both exponential and linear material variations are considered. First, analytical solutions for stresses and displacements are developed for orthotropic FGMs and, afterwards, they are particularized (e.g., in the limit) for isotropic FGMs. The analytical solutions for exponentially graded isotropic FGMs coincide with those of Erdogan and Wu

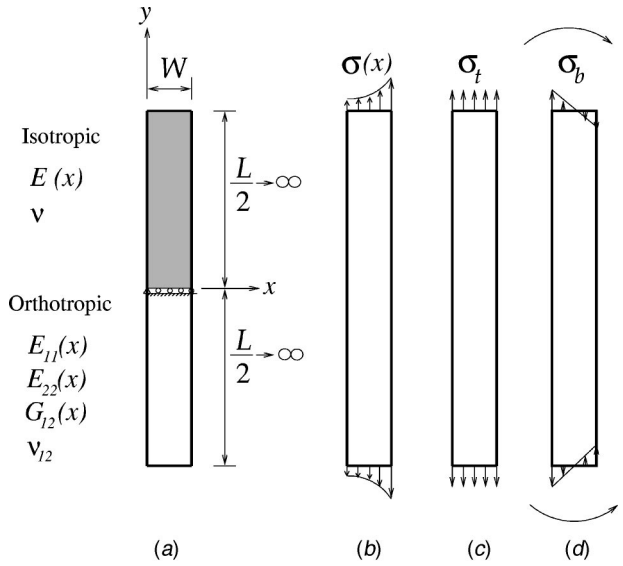

Fig. 4 An isotropic or orthotropic functionally graded plate: (*a*) geometry and material properties—the shaded portion indicates the symmetric region of the plate used in this analysis; (*b*) fixed grip loading with a schematic of the corresponding stresses at the end points of the plate; (*c*) tension loading; (*d*) bending loading

([32]) and Paulino and Kim ([33]). The analytical solutions for linearly graded isotropic and orthotropic FGMs are new solutions derived in this work.

2.1 Exponential Material Variation. Consider a plate under generalized plane stress conditions (see Fig. 4) made of a nonhomogeneous orthotropic material. Assume the Poisson's ratio

(ν_{12}) constant, and the Young's moduli and in-plane shear modulus with variations given by the following expressions:

$$\begin{aligned} E_{11}(x) &= E_{11}^0 e^{\beta_{11}x} \\ E_{22}(x) &= E_{22}^0 e^{\beta_{22}x} \\ G_{12}(x) &= G_{12}^0 e^{\beta_{12}x} \\ \nu_{12}(x) &= \text{constant}, \end{aligned} \tag{3}$$

where $E_{11}^0 = E_{11}(0)$, $E_{22}^0 = E_{22}(0)$, and $G_{12}^0 = G_{12}(0)$ are the material properties at the $x=0$ line (see Fig. 4(*a*)), and the coefficients β_{ij} above are independent nonhomogeneity parameters characterized by

$$\begin{aligned} \beta_{11} &= \frac{1}{W}\log\left[\frac{E_{11}(W)}{E_{11}(0)}\right] \\ \beta_{22} &= \frac{1}{W}\log\left[\frac{E_{22}(W)}{E_{22}(0)}\right] \\ \beta_{12} &= \frac{1}{W}\log\left[\frac{G_{12}(W)}{G_{12}(0)}\right], \end{aligned} \tag{4}$$

where W is the width of the FGM plate as shown in Fig. 4. Notice that in this case the β_{ij} parameters have units $[Length]^{-1}$.

For a corresponding nonhomogeneous isotropic material ($E = E_{11} = E_{22}$, $G = G_{12}$, $\nu_{12} = \nu$), the Poisson's ratio is assumed constant and the Young's modulus varies exponentially, i.e.,

$$\begin{aligned} E(x) &= E^0 e^{\beta x} \\ \nu(x) &= \text{constant} \end{aligned} \tag{5}$$

where $E^0 = E(0)$. The nonhomogeneity parameter β is given by

$$\beta = \frac{1}{W}\log\left[\frac{E(W)}{E(0)}\right] \tag{6}$$

which has units $[Length]^{-1}$.

2.1.1 Fixed Grip Loading. For fixed grip loading (see Fig. 4(*b*)) with $\varepsilon_{yy}(x, \pm\infty) = \varepsilon_0$, the stress distribution becomes

$$\sigma_{yy}(x) = E_{22}^0 \varepsilon_0 e^{\beta_{22}x}. \tag{7}$$

Using strain-displacement relations and the boundary conditions

$$u_x(0,0) = 0, \quad u_y(x,0) = 0, \tag{8}$$

one obtains the displacements

$$\begin{aligned} u_x(x,y) &= -\nu_{12}\varepsilon_0 \frac{E_{22}^0}{E_{11}^0}\frac{1}{\beta_{22}-\beta_{11}}\left[e^{(\beta_{22}-\beta_{11})x}-1\right] \\ u_y(x,y) &= \varepsilon_0 y. \end{aligned} \tag{9}$$

Notice that for isotropic materials ($E = E_{11} = E_{22}$, $G_{12} = G$, and $\nu_{12} = \nu$), the stress distribution (7) becomes ([32])

$$\sigma_{yy}(x) = E^0 \varepsilon_0 e^{\beta x} \tag{10}$$

and the displacements are obtained in the limit of Eq. (9) as $(\beta_{22}-\beta_{11}) \to 0$. Thus ([33])

$$\begin{aligned} u_x(x,y) &= -\nu\varepsilon_0 x \\ u_y(x,y) &= \varepsilon_0 y. \end{aligned} \tag{11}$$

2.1.2 Tension and Bending. For tension and bending loads (see Figs. 4(*c*) and 4(*d*), respectively), the applied stresses are defined by

$$N = \sigma_t W, \quad M = \frac{\sigma_b W^2}{6}, \tag{12}$$

where N is a membrane resultant along the $x = W/2$ line (see Fig. 4(*a*)), and M is the bending moment. For these two loading cases, the compatibility condition $\partial^2 \varepsilon_{yy}/\partial x^2 = 0$ gives $\varepsilon_{yy} = Ax + B$ and thus

$$\sigma_{yy}(x) = E_{22}^0 e^{\beta_{22}x}(Ax + B) \tag{13}$$

where the constants A (with unit $[Length]^{-1}$) and B (dimensionless) are determined from

$$\int_0^W \sigma_{yy}(x)\,dx = N, \quad \int_0^W \sigma_{yy}(x)\,x\,dx = M \tag{14}$$

by assuming

$$\begin{aligned} M &= NW/2 \quad \text{for tension} \\ N &= 0 \quad \text{for bending.} \end{aligned} \tag{15}$$

Thus, for tension load, the stress distribution is given by Eq. (13) with

$$\begin{aligned} A &= \frac{\beta_{22}N}{2E_{22}^0}\left(\frac{W\beta_{22}^2 e^{\beta_{22}W} - 2\beta_{22}e^{\beta_{22}W} + W\beta_{22}^2 + 2\beta_{22}}{e^{\beta_{22}W}\beta_{22}^2W^2 - e^{2\beta_{22}W} + 2e^{\beta_{22}W} - 1}\right), \\ B &= \frac{\beta_{22}N}{2E_{22}^0}\left(\frac{e^{\beta_{22}W}[e^{\beta_{22}W}(-W^2\beta_{22}^2 + 3\beta_{22}W - 4) + W^2\beta_{22}^2 - 2\beta_{22}W + 8] - \beta_{22}W - 4}{(e^{\beta_{22}W}-1)(e^{\beta_{22}W}\beta_{22}^2W^2 - e^{2\beta_{22}W} + 2e^{\beta_{22}W} - 1)}\right). \end{aligned} \tag{16}$$

For bending load, the stress distribution is also given by Eq. (13), however, the coefficients A and B for this case are

$$\begin{aligned} A &= \frac{\beta_{22}^2 M}{E_{22}^0}\left(\frac{\beta_{22}(1-e^{\beta_{22}W})}{e^{\beta_{22}W}\beta_{22}^2W^2 - e^{2\beta_{22}W} + 2e^{\beta_{22}W} - 1}\right), \\ B &= \frac{\beta_{22}^2 M}{E_{22}^0}\left(\frac{\beta_{22}We^{\beta_{22}W} - e^{\beta_{22}W} + 1}{e^{\beta_{22}W}\beta_{22}^2W^2 - e^{2\beta_{22}W} + 2e^{\beta_{22}W} - 1}\right), \end{aligned} \tag{17}$$

respectively. For both tension and bending loads, using the strain-displacement relations and the boundary conditions (8), one obtains the displacements

$$\begin{aligned} u_x(x,y) &= -\nu_{12}\frac{E_{22}^0}{E_{11}^0}\left\{\frac{\left(Ax - \dfrac{A}{\beta_{22}-\beta_{11}} + B\right)}{\beta_{22}-\beta_{11}}e^{(\beta_{22}-\beta_{11})x}\right. \\ &\quad \left. + \frac{A - B(\beta_{22}-\beta_{11})}{(\beta_{22}-\beta_{11})^2}\right\} - \frac{A}{2}y^2 \\ u_y(x,y) &= (Ax + B)y. \end{aligned} \tag{18}$$

The constants A and B refer to the appropriate loading case above, either tension (Eq. (16)) or bending (Eq. (17)).

For the isotropic case ($E=E_{11}=E_{22}$, $G_{12}=G$, and $\nu_{12}=\nu$), the stress distribution is obtained by Eqs. (16) and (17) (for tension and bending loads, respectively) with β_{22} replaced by β, which agree with Erdogan and Wu's [32] solution. The displacements are obtained in the limit of Eq. (18) as $(\beta_{22}-\beta_{11})\to 0$. Thus ([33])

$$u_x(x,y)=\nu\left(\frac{A}{2}x^2+Bx\right)-\frac{A}{2}y^2$$
$$u_y(x,y)=(Ax+B)y. \tag{19}$$

2.2 Linear Material Variation. Once again, consider a plate under generalized plane stress conditions, as illustrated by Fig. 4. Assume the Poisson's ratio (ν_{12}) is constant, and the Young's moduli and in-plane shear modulus with variations given by the following expressions (cf. Eq. (3)):

$$E_{11}(x)=E_{11}^0+\gamma_{11}x$$
$$E_{22}(x)=E_{22}^0+\gamma_{22}x$$
$$G_{12}(x)=G_{12}^0+\gamma_{12}x \tag{20}$$
$$\nu_{12}(x)=\text{constant},$$

where $E_{11}^0=E_{11}(0)$, $E_{22}^0=E_{22}(0)$, and $G_{12}^0=G_{12}(0)$ are the material properties at the $x=0$ line (see Fig. 4(a)) and the coefficients γ_{ij} are independent nonhomogeneity parameters characterized by

$$\gamma_{11}=\frac{E_{11}(W)-E_{11}(0)}{W}$$
$$\gamma_{22}=\frac{E_{22}(W)-E_{22}(0)}{W} \tag{21}$$
$$\gamma_{12}=\frac{G_{12}(W)-G_{12}(0)}{W}.$$

Notice that in this case the γ_{ij} parameters have units $[Force]/[Length]^3$.

For a corresponding nonhomogeneous isotropic material ($E=E_{11}=E_{22}$, $G=G_{12}$, $\nu_{12}=\nu$), the Poisson's ratio is assumed constant and the Young's modulus varies linearly, i.e.,

$$E(x)=E^0+\gamma x$$
$$\nu(x)=\text{constant} \tag{22}$$

where $E^0=E(0)$. The nonhomogeneity parameter γ is given by

$$\gamma=\frac{E(W)-E(0)}{W} \tag{23}$$

which has units $[Force]/[Length]^3$.

2.2.1 Fixed Grip Loading. For fixed grip loading (see Fig. 4(b)) with $\varepsilon_{yy}(x,\pm\infty)=\varepsilon_0$, the stress distribution becomes

$$\sigma_{yy}(x)=\varepsilon_0(E_{22}^0+\gamma_{22}x). \tag{24}$$

Using strain-displacement relations and the boundary conditions.

$$u_x(0,0)=0,\quad u_y(x,0)=0,$$

one obtains the displacements

$$u_x(x,y)=-\nu_{12}\varepsilon_0\left\{\frac{\gamma_{22}}{\gamma_{11}}x+\frac{E_{22}^0\ln(E_{11}^0+\gamma_{22}x)}{\gamma_{11}}\right.$$
$$-\frac{\gamma_{22}E_{11}^0\ln(E_{11}^0+\gamma_{11}x)}{\gamma_{11}^2}$$
$$\left.-\left(\frac{E_{22}^0}{\gamma_{11}}-\frac{\gamma_{22}E_{11}^0}{\gamma_{11}^2}\right)\ln(E_{11}^0)\right\}$$
$$u_y(x,y)=\varepsilon_0 y. \tag{25}$$

For isotropic materials ($E=E_{11}=E_{22}$, $G_{12}=G$, and $\nu_{12}=\nu$), the stress distribution (24) becomes

$$\sigma_{yy}(x)=\varepsilon_0(E^0+\gamma x), \tag{26}$$

and the displacements are obtained from Eq. (25) as

$$u_x(x,y)=-\nu\varepsilon_0 x$$
$$u_y(x,y)=\varepsilon_0 y. \tag{27}$$

2.2.2 Tension and Bending. For tension and bending loads (see Fig. 4(c) and 4(d), respectively), the applied stresses are defined by Eq. (12), i.e.,

$$N=\sigma_t W,\quad M=\frac{\sigma_b W^2}{6},$$

where N is a membrane resultant applied along the $x=W/2$ line (see Fig. 4(a)), and M is the bending moment. For these two loading cases, the compatibility condition $\partial^2\varepsilon_{yy}/\partial x^2=0$ gives $\varepsilon_{yy}=Ax+B$ and thus

$$\sigma_{yy}(x)=(E_{22}^0+\gamma_{22}x)(Ax+B), \tag{28}$$

where the constants A (with unit $[Length]^{-1}$) and B (dimensionless) are determined from Eq. (14), i.e.,

$$\int_0^W\sigma_{yy}(x)dx=N,\quad \int_0^W\sigma_{yy}(x)x\,dx=M,$$

by assuming (see Eq. (15))

$$M=NW/2\quad \text{for tension}$$
$$N=0\quad \text{for bending}. \tag{29}$$

Thus, for tension load, the stress distribution is given by Eq. (28) with

$$A=\frac{-\gamma_{22}N}{\frac{1}{6}\gamma_{22}^2W^3+\gamma_{22}E_{22}^0W^2+(E_{22}^0)^2W},$$
$$B=\frac{N(E_{22}^0+\gamma_{22}W)}{\frac{1}{6}\gamma_{22}^2W^3+\gamma_{22}E_{22}^0W^2+(E_{22}^0)^2W}. \tag{30}$$

For bending load, the stress distribution is also given by Eq. (28) with

$$A=\frac{-36M(2E_{22}^0+\gamma_{22}W)}{\gamma_{22}^2W^5+6E_{22}^0\gamma_{22}W^4+6(E_{22}^0)^2W^3},$$
$$B=\frac{36M(2E_{22}^0+\gamma_{22}W)}{\gamma_{22}^2W^5+6E_{22}^0\gamma_{22}W^4+6(E_{22}^0)^2W^3}\frac{3\gamma_{22}W^2+3E_{22}^0W}{2\gamma_{22}W+6E_{22}^0}. \tag{31}$$

For both tension and bending loads, using the strain-displacement relations and the boundary conditions.

$$u_x(0,0)=0,\ u_y(x,0)=0,$$

one obtains the displacements in closed form, which are given by

$$u_x(x,y)=-\nu_{12}\left\{-\left(\frac{E_{11}^0\gamma_{22}A}{\gamma_{11}^2}-\frac{\gamma_{22}B}{\gamma_{11}}-\frac{E_{22}^0A}{\gamma_{11}}\right)x+\frac{\gamma_{22}A}{2\gamma_{11}}x^2+\left(\frac{E_{22}^0B}{\gamma_{11}}-\frac{E_{11}^0\gamma_{22}B}{\gamma_{11}^2}-\frac{E_{11}^0E_{22}^0A}{\gamma_{11}^2}+\frac{(E_{11}^0)^2\gamma_{22}A}{\gamma_{11}^3}\right)\ln(\gamma_{11}x+E_{11}^0)\right.$$
$$\left.-\left(\frac{E_{22}^0B\gamma_{11}^2-E_{11}^0\gamma_{11}\gamma_{22}B-E_{11}^0E_{22}^0\gamma_{11}A+(E_{11}^0)^2\gamma_{22}A}{\gamma_{11}^3}\right)\ln(E_{11}^0)\right\}-\frac{A}{2}y^2,$$
$$u_y(x,y)=(Ax+B)y. \tag{32}$$

For the isotropic case ($E=E_{11}=E_{22}$, $G_{12}=G$, and $\nu_{12}=\nu$), the stress distribution is obtained by Eqs. (30) and (31) (for tension and bending loads, respectively) with γ_{22} and E_{22}^0, replaced by γ and E^0, respectively. The displacements are obtained from Eq. (32) as

$$u_x(x,y)=\nu\left(\frac{A}{2}x^2+Bx\right)-\frac{A}{2}y^2$$
$$u_y(x,y)=(Ax+B)y. \tag{33}$$

Notice that the form of the exact solutions for displacements in orthotropic FGMs differs significantly from that for isotropic FGMs because the former case depend on two principal Young's moduli, while in the latter case the explicit moduli dependence is absent.

3 Basic Finite Element Formulation

Displacements for an isoparametric finite element can be written as

$$\boldsymbol{u}^e=\sum_{i=1}^{m}N_i\boldsymbol{u}_i^e \tag{34}$$

where N_i are shape functions, $\boldsymbol{u}_i$ is the nodal displacement corresponding to node i, and m is the number of nodal points in the element. For example, for a Q4 element, the standard shape functions are

$$N_i=(1+\xi\xi_i)(1+\eta\eta_i)/4,\quad i=1,\ldots,4 \tag{35}$$

where (ξ,η) denote intrinsic coordinates in the interval $[-1,1]$ and (ξ_i,η_i) denote the local coordinates of node i. As usual, strains are obtained from displacements by differentiation as.

$$\boldsymbol{\varepsilon}^e=\boldsymbol{B}^e\boldsymbol{u}^e \tag{36}$$

where $\boldsymbol{B}^e$ is the strain-displacement matrix of shape function derivatives, and $\boldsymbol{u}^e$ is the nodal displacement vector. Thus strain-stress relations are given by

$$\boldsymbol{\sigma}^e=\boldsymbol{D}^e(\boldsymbol{x})\boldsymbol{\varepsilon}^e \tag{37}$$

where $\boldsymbol{D}^e(\boldsymbol{x})$ is the constitutive matrix, which is a function of position for nonhomogeneous materials, i.e., $\boldsymbol{D}^e(\boldsymbol{x})=\boldsymbol{D}^e(x,y)$. The principle of virtual work (PVW) yields the following finite element stiffness equations ([34])

$$\boldsymbol{k}^e\boldsymbol{u}^e=\boldsymbol{F}^e \tag{38}$$

where $\boldsymbol{F}^e$ is the load vector and the element stiffness matrix is

$$\boldsymbol{k}^e=\int_{\Omega_e}\boldsymbol{B}^{e^T}\boldsymbol{D}^e(\boldsymbol{x})\boldsymbol{B}^e d\Omega_e \tag{39}$$

in which Ω_e is the domain of element (e), and T denotes transpose. The reasoning above, at the element level, can be readily extended to the whole domain, which leads to a system of algebraic equations for the unknown displacements ([34]).

4 Generalized Isoparametric Graded Finite Elements

For simplicity of notation, the superscript (e), denoting the element, is dropped in this section. Material properties (e.g., at each Gaussian integration point) can be interpolated from the nodal material properties of the element using isoparametric shape functions which are the same for spatial coordinates (x,y):

$$x=\sum_{i=1}^{m}N_ix_i,\quad y=\sum_{i=1}^{m}N_iy_i \tag{40}$$

and displacements (u,v):

$$u=\sum_{i=1}^{m}N_iu_i,\quad v=\sum_{i=1}^{m}N_iv_i. \tag{41}$$

Thus, by generalization of the isoparametric concept, the Young's modulus $E=E(\boldsymbol{x})$ and Poisson's ratio $\nu=\nu(\boldsymbol{x})$ are interpolated as

$$E=\sum_{i=1}^{m}N_iE_i,\quad \nu=\sum_{i=1}^{m}N_i\nu_i \tag{42}$$

respectively, as illustrated by Fig. 5. Similar expansions can also be made to two-dimensional orthotropic materials where the four independent engineering elastic parameters are the principal Young's moduli, $E_{11}\equiv E_{11}(\boldsymbol{x})$, $E_{22}\equiv E_{22}(\boldsymbol{x})$, in-plane shear modulus $G_{12}\equiv G_{12}(\boldsymbol{x})$; and Poisson's ratio $\nu_{12}=\nu_{12}(\boldsymbol{x})$, i.e.,

$$E_{11}=\sum_{i=1}^{m}N_i(E_{11})_i,\quad E_{22}=\sum_{i=1}^{m}N_i(E_{22})_i,$$
$$G_{12}=\sum_{i=1}^{m}N_i(G_{12})_i,\quad \nu_{12}=\sum_{i=1}^{m}N_i(\nu_{12})_i, \tag{43}$$

as illustrated by Fig. 5.

Some material models may be given in terms of the volume fraction (V) of a material phase, "p," e.g., the metal phase in a ceramic/metal FGM ([35]). In this case, the generalized isoparametric formulation consists of approximating V^p by the standard interpolation

$$V^p=\sum_{i=1}^{m}N_iV_i^p \tag{44}$$

where V_i^p $(i=1,2,\ldots,m)$ are the values of V^p at the nodal points. This approach offers a convenient framework to couple the finite

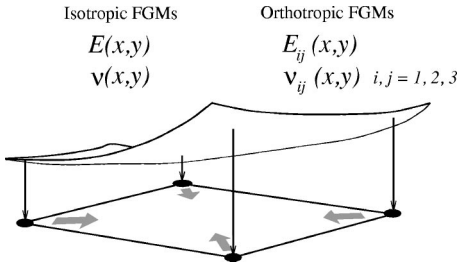

Fig. 5 Generalized isoparametric formulation for isotropic or orthotropic FGMs

element method with micromechanics-based models, e.g., self-consistent scheme.

The above framework allows development of a fully isoparametric formulation in the sense that the same shape functions are used to interpolate the unknown displacements, the geometry, and the material properties. Thus, the actual variation of the material properties may be approximated by the element interpolation functions (e.g., a certain degree of polynomial functions).

5 Numerical Examples

Although the finite element method offers a lot of flexibility in terms of modeling material property variation, the actual choice of properties and boundary value problems in this section was dictated by the analytical solutions derived in Section 2 for the plate configuration of Fig. 4. Here the analytical solutions are compared with the numerical ones. The examples are divided into two groups:

1. isotropic FGM plate
2. orthotropic FGM plate

For each group, two material variations along the Cartesian direction x are examined:

1. exponentially graded materials
2. linearly graded materials

and also the following loading conditions are considered:

1. fixed grip
2. tension loading
3. bending loading

The relevant stress values obtained numerically by the finite element method are compared with the analytical results. For fixed grip loading (see Fig. 4(b)), the stress σ_{yy} is considered. For tension applied parallel to the material gradation, the stress σ_{xx} is the quantity of interest, while for tension and bending loads applied perpendicular to the material gradation (see Figs. 4(c) and 4(d), respectively), the stress σ_{yy} is the relevant quantity. Moreover, for a few of the examples, the displacements computed numerically are also compared with the analytical results.

The finite element meshes consist of square elements (Q4 or Q8) with edges of unit length. For all the examples, 2×2 Gauss quadrature was employed. All the numerical stress values reported here are nodal values extrapolated directly from the Gauss points and without any averaging. The finite element program developed in this work was implemented by the authors in a simple code using MATLAB.

5.1 Isotropic Functionally Graded Plate. Figure 6 illustrates an isotropic FGM plate with material variation in the Cartesian direction x subjected to various loading conditions. Figure 6(a) shows the basic geometry, boundary conditions and properties. The finite element mesh consists of 9×9 Q4 or Q8 elements (either graded or homogeneous) as illustrated in Figs. 6(b) to 6(d). The Young's modulus varies from

$$E_1=E^0=E(0) \quad \text{to} \quad E_2=E(W) \tag{45}$$

either exponentially as given by Eq. (5) or linearly as given by Eq. (22) with $E_1=1.0$ and $E_2=8.0$. The independent nonhomogeneity parameters are given by Eqs. (6) and (23) for the exponential and linear material variations, respectively, with

$$\beta=(\ln(8/1))/9 \quad \text{and} \quad \gamma=7/9. \tag{46}$$

Consistent units are employed here. The Poisson's ratio is constant and it is selected as follows:

$\nu=0.3$ for tension and bending applied perpendicular to material gradation (Figs. 6(b) and 6(c), respectively)

$\nu=0.0$ for tension load parallel to material gradation (Fig. 6(d)).

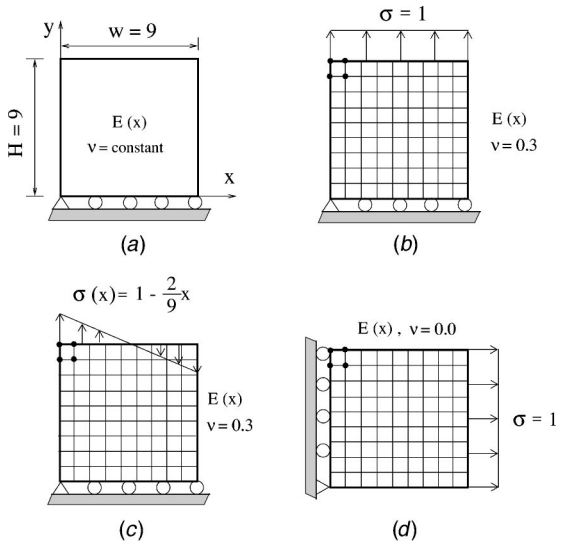

Fig. 6 Isotropic FGM plate with material variation in the x-direction: (a) geometry, boundary conditions and material properties; (b) tension load perpendicular to material gradation; (c) bending load; (d) tension load parallel to material gradation. The finite element mesh (9×9 quads: either Q4 or Q8) is illustrated in parts (b) through (d) with a representative Q4 element at the upper left hand corner

The behavior of the elements (homogeneous versus graded) is as follows. Figure 7 shows the stress σ_{yy} versus x for an exponentially graded isotropic plate subjected to a uniform displacement in the y direction with $\varepsilon_0=\Delta/H$. According to Eq. (10), the stress σ_{yy} is uniform in the y-direction and thus the graph of Fig. 7 is applicable to the entire range of y coordinates, i.e., $0\leqslant y\leqslant H$ (see Fig. 6(a)). In this case, the solution obtained with graded Q4 elements matches the exact solution. This is expected because the exact displacement field is linear (see Eq. (11) and Fig. 8), which is captured by linear isoparametric elements such as Q4. Moreover, because of the linearity of the analytical solution (Eq. (11)), a single Q4 element could be used to predict the exact solution. Figure 7 also shows that the stress obtained with homogeneous Q4 elements is piecewise constant due to the fact that these elements have a single value for each material property, which leads to a piecewise constant material property approximation as illustrated by Fig. 1. Therefore such homogeneous elements predict the actual stress values only at their centroids where

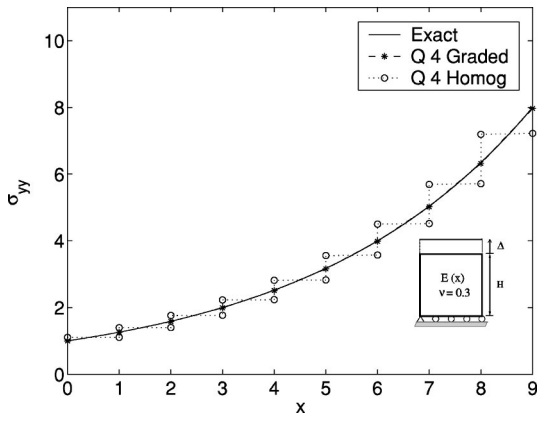

Fig. 7 Stress distribution (σ_{yy}) using Q4 elements for *fixed grip* ($\varepsilon_0=\Delta/H$) load applied perpendicular to the *exponential* material gradation

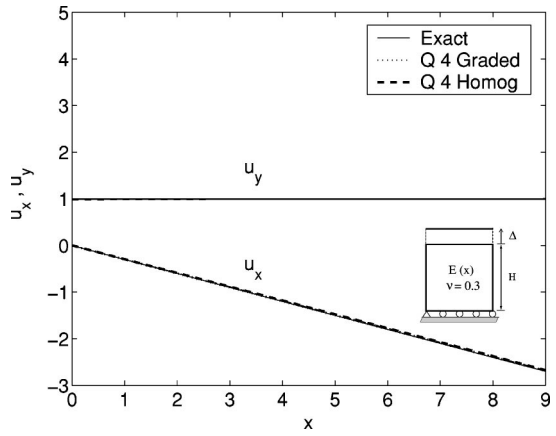

Fig. 8 Displacements (u_x and u_y) using Q4 elements for *fixed grip* load applied perpendicular to the *exponential* material gradation in isotropic FGMs

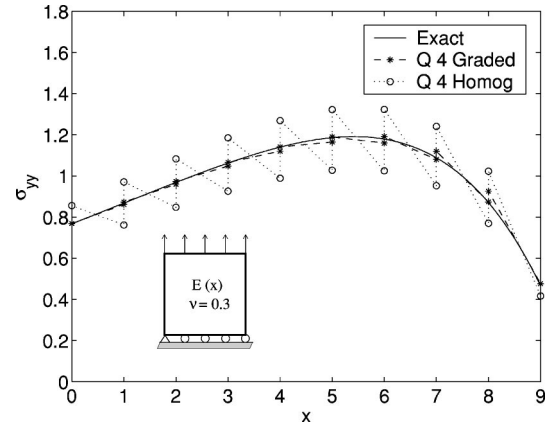

Fig. 9 Stress distribution (σ_{yy}) using Q4 elements for *tension* load applied perpendicular to the *exponential* material gradation

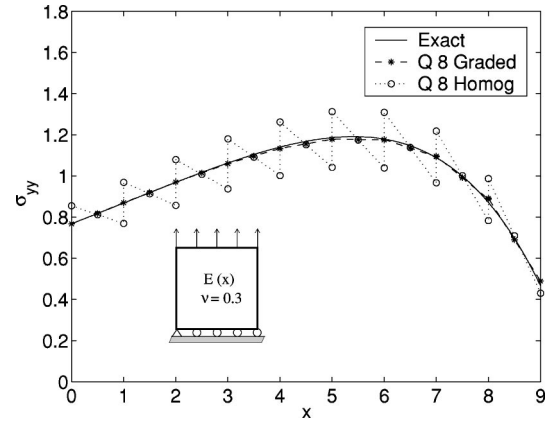

Fig. 10 Stress distribution (σ_{yy}) using Q8 elements for *tension* load applied perpendicular to the *exponential* material gradation

the properties match the material gradation. Moreover, the amplitude of the nodal stress jumps for homogeneous Q4 elements increases with coordinate x in a nearly exponential fashion, as illustrated by Fig. 7. These observations are consistent with those by Santare and Lambros ([30]). Of course, the exact solution is also recovered with higher-order graded elements, e.g., Q8. The homogeneous Q8 elements also lead to a piecewise constant nodal

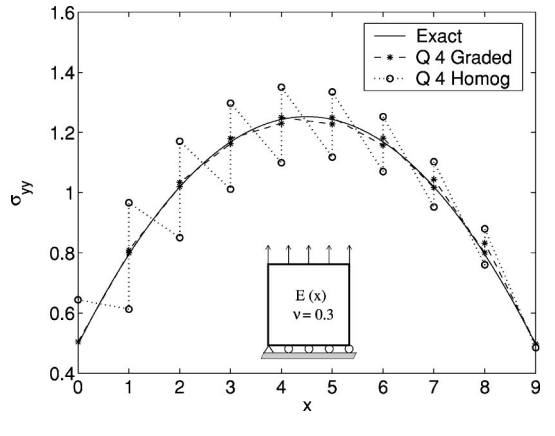

Fig. 11 Stress distribution (σ_{yy}) using Q4 elements for *tension* loading applied perpendicular to the *linear* material gradation

stress profile with the stress at the midnode location along the x direction matching the exact stress value, which occurs because the material properties at the mid-nodes match the actual material properties.

Figures 9 and 10 compare nodal stresses interpolated from stresses at Gauss integration points using graded and homogeneous Q4 and Q8 elements, respectively, which are subjected to tension loading applied perpendicular to the material gradation. Figures 11 and 12 show such comparison considering linear material variation. On the left side of the domain in Figs. 9–12, the exact solution shows an increasing trend of σ_{yy} with x, while the homogeneous elements (either Q4 or Q8) give σ_{yy} as a decreasing function of x in each individual element. Notice that this problem does not occur with the graded elements. In this case, the exact solution for displacements is quadratic (see Eqs. (19) and (33) for exponential and linear material variations, repectively), which coincides with the order of interpolation for the Q8 element. Moreover, the material variation for the linear case is captured by the element shape functions. The stress results for the Q8 element considering exponential and linear material variations are shown in Figs. 10 and 12, respectively. As expected, the homogeneous Q8 element shows piecewise variation while the graded Q8 element approaches the analytical solution quite well. The relatively small differences observed between the analytical and graded Q8 solutions may be attributed to the finite plate length (length/

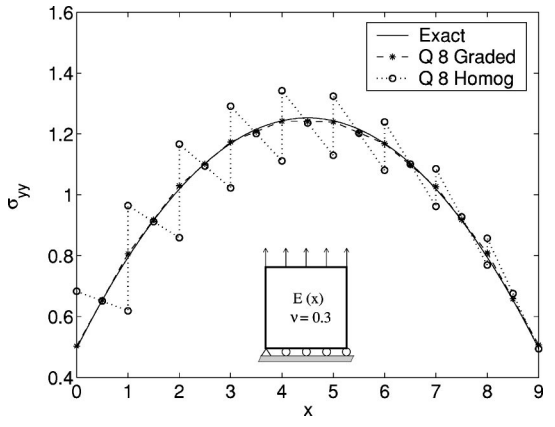

Fig. 12 Stress distribution (σ_{yy}) using Q8 elements for *tension* load applied perpendicular to the *linear* material gradation

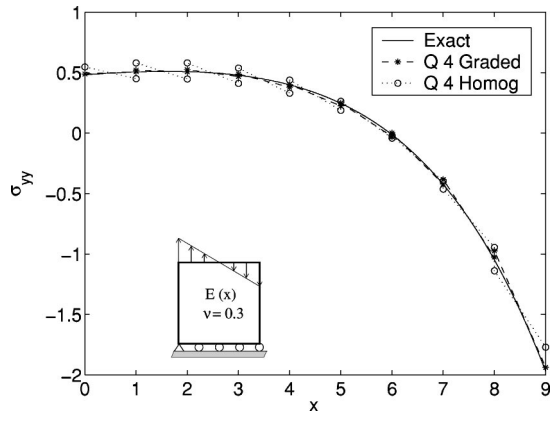

Fig. 13 Stress distribution (σ_{yy}) using Q4 elements for *bending* load applied perpendicular to the *exponential* material gradation

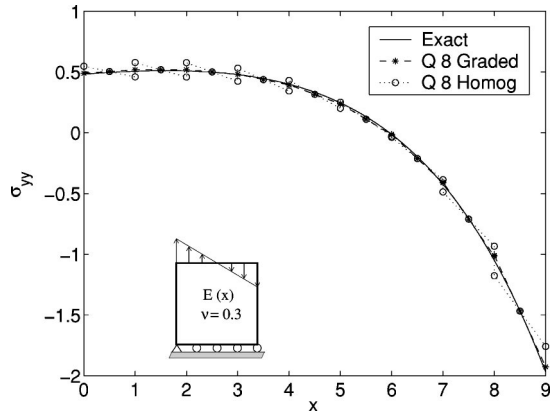

Fig. 14 Stress distribution (σ_{yy}) using Q8 elements for *bending* load applied perpendicular to the *exponential* material gradation

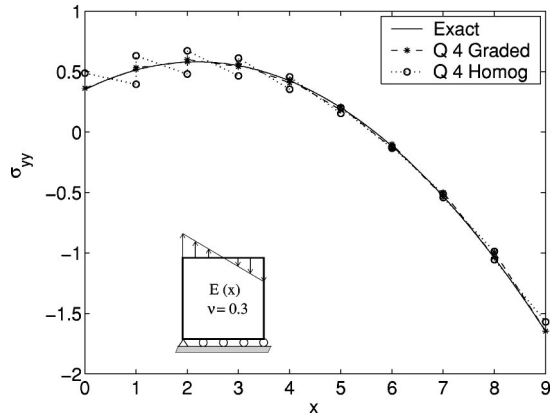

Fig. 15 Stress distribution (σ_{yy}) using Q4 elements for *bending* load applied perpendicular to the *linear* material gradation

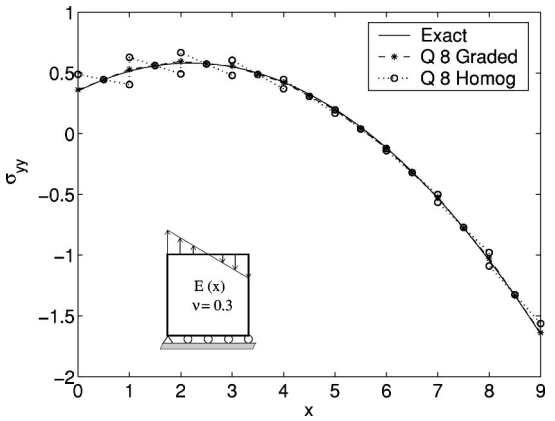

Fig. 16 Stress distribution (σ_{yy}) using Q8 elements for *bending* load applied perpendicular to the *linear* material gradation

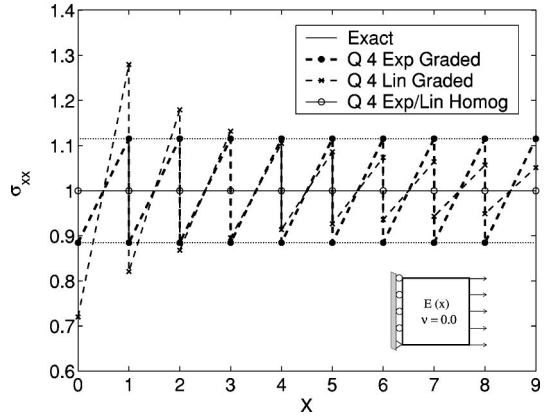

Fig. 17 Stress distribution (σ_{xx}) using Q4 elements (9×9 mesh) for *tension* load applied parallel to the *exponential* or *linear* material gradation

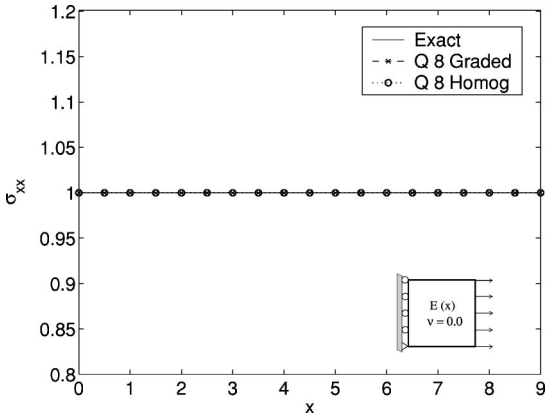

Fig. 18 Stress distribution (σ_{xx}) using Q8 elements (9×9 mesh) for *tension* load applied parallel to the *material* gradation

width=1 as shown in Fig. 6) utilized in the numerical calculation—the analytical solution was derived for an *infinitely long* plate of finite width.

A similar comparison is also made for a different loading case consisting of bending applied perpendicular to the material gradation. Figures 13 and 14 show the behavior of the Q4 and Q8 elements, respectively, for the exponential variation. Figures 15 and 16 show such comparison for the bending case considering linear material variation. The stress results for the Q8 element considering exponential and linear material variations are shown in Figs. 14 and 16, respectively. Similar comments to those made comparing the Q8 (homogeneous versus graded) and analytical solutions for the tension load case also hold for the present bending load case.

The above results lead to the following observations. The variation of stress with position x is larger for linear than with exponential material variations (cf. Figs. 9 and 11, 10 and 12, 13 and 15, and 14 and 16). In general, the amplitude of stress jumps between Q4 elements is larger than between Q8 elements, especially for conventional homogeneous elements (cf. Figs. 9 and 10,

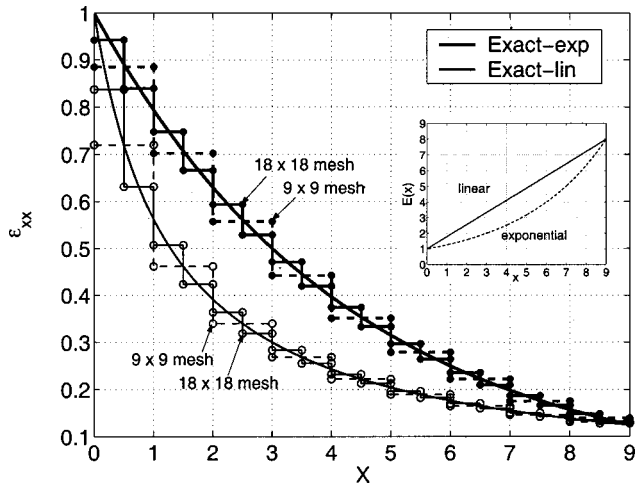

Fig. 19 Strain distribution (ε_{xx}) using Q4 elements (either 9×9 and 18×18) for *tension* load applied parallel to the material gradation (either exponential or linear)

11 and 12, 13 and 14, 15 and 16, and 17 and 18). As expected, the graded elements show superior performance to homogeneous elements, i.e., the graded elements provide a better approximation to the exact solution in every element. Essentially, the graded elements show good performance in terms of actual (i.e., no averaging) nodal stress (σ_{yy}) along the $y=0$ line and the homogeneous elements behave well in terms of the averaged nodal stresses.

Figures 17 and 18 compare nodal stresses of graded versus homogeneous Q4 and Q8 elements (9×9 mesh), respectively, which are subjected to tension applied parallel to the material gradation (see Fig. 6(*d*)). The exact solution is $\sigma_{xx}=1.0$. Different from the observation above, it is interesting to observe in Fig. 17 that the Q4 graded element shows poor performance when compared to Q4 homogeneous elements for both material variations (i.e., exponential and linear). Although mesh refinement (for a fixed material gradient) increases the accuracy of the solution, the same trend of Fig. 17 is observed for a finer mesh, e.g., 18×18. Figure 17 shows that the Q4 graded elements provide piecewise continuous solutions to the nodal stresses (σ_{xx}), while the homogeneous Q4 elements do recover the exact solution. This is the reverse of the effect seen in the previous load cases. However, a higher order element such as Q8 (either graded or homogeneous) is able to capture the exact solution in this case, as shown in Fig. 18.

A few additional remarks, regarding the behavior of Q4 elements observed in Fig. 17, are in order. Both graded and homogeneous elements lead to the same displacements at all nodes and the same constant strains for each element. Notice that along the $y=0$ line, the nodal stress range has constant amplitude for the exponential material case, while it has decreasing amplitude for the linear material case (see Fig. 17). The reason for this behavior is illustrated by Fig. 19 by investigating the strain distribution for two mesh discretizations (9×9 and 18×18 meshes). For instance, for the exponential material case, the nodal strains decrease exponentially while the Young's modulus increase exponentially. Thus the multiplication of these two factors cancel each other to give a constant stress amplitude at the nodal points, as shown in Fig. 17.

5.2 Orthotropic Functionally Graded Plate. Figure 20 shows orthotropic FGM plates, with material variation in the Cartesian direction *x*, subjected to various loading conditions. Figure 20(*a*) shows the basic geometry, boundary conditions and material property variation. The two principal Young's moduli and in-plane shear modulus vary proportionally either with an exponential function of *x* as given by Eq. (3) or with a linear function of *x* as

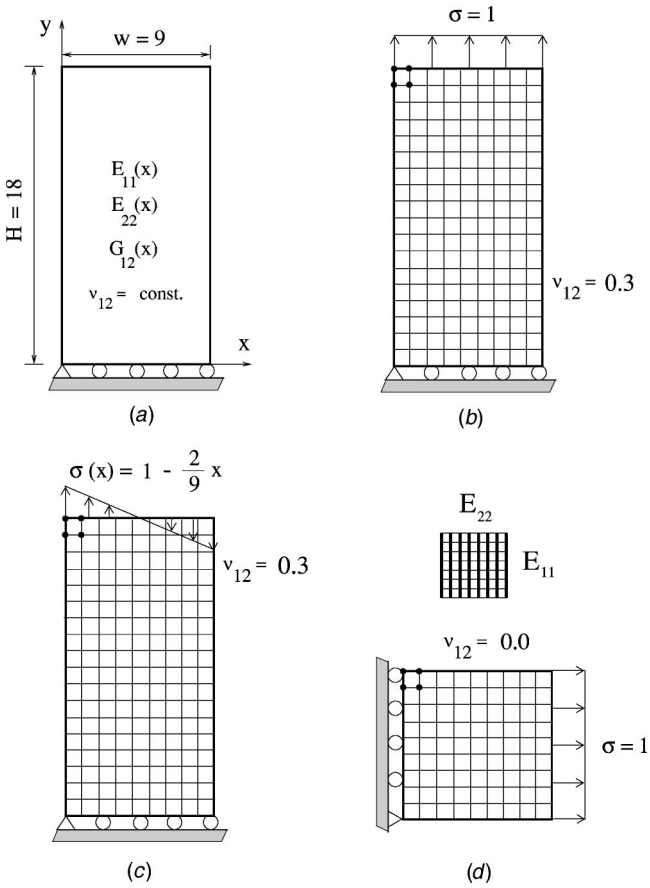

Fig. 20 Orthotropic FGM plate with material variation in the *x*-direction: (*a*) geometry, boundary conditions and material properties; (*b*) tension load perpendicular to material gradation; (*c*) bending load; (*d*) tension load parallel to the material gradation. The finite element mesh (Q4 or Q8 elements) is illustrated in parts (*b*) through (*d*) with a representative Q4 element at the upper left hand corner

given by Eq. (20). The independent nonhomogeneity parameters (β_{ij} and γ_{ij}) are given by Eqs. (4) and (21) for the exponential and linear material variations, respectively. The Poisson's ratio is assumed constant.

For the examples in Fig. 20, the finite element mesh consists of either Q4 or Q8 (graded or homogeneous) elements under generalized plane stress. The mesh for the geometry of Figs. 20(*b*) and 20(*c*) consists of 9×18 elements. For the sake of completeness, all the properties used in the numerical analyses are given as follows. However, due to space limitations, not all the results are shown here, but they are reported elsewhere ([36]). For the fixed grip case and for tension and bending perpendicular to the material gradation, the following data were used for the finite element analysis:

$$E_{11}^0=1, \quad E_{22}^0=0.1, \quad G_{12}^0=0.5, \quad \nu_{12}=0.3$$

in which consistent units are employed. For tension parallel to the material gradation, the following data were used for the finite element analysis:

$$E_{11}^0=1, \quad E_{22}^0=0.1, \quad G_{12}^0=0.5, \quad \nu_{12}=0.0.$$

For the single case of fixed grip loading, only exponential material variation was considered. In this case, the β_{ij} parameters are

$$\beta_{22}=(\ln 8)/9=\beta, \quad \beta_{11}=\beta/2, \quad \beta_{12}=\beta/3$$

so that the range of properties is the following

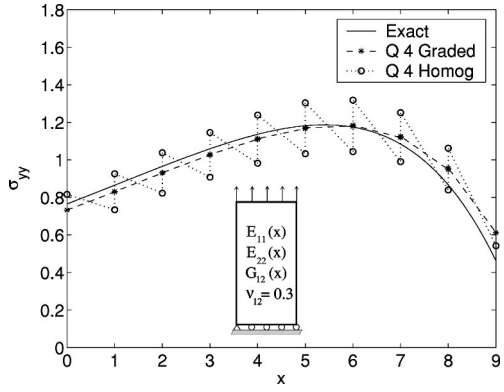

Fig. 21 Stress distribution (σ_{yy}) using Q4 elements for *tension* loading applied perpendicular to the *exponential* material gradation in orthotropic FGMs ($E_{11}^0=1$, $E_{22}^0=0.1$, $G_{12}^0=0.5$, $\nu_{12}=0.3$)

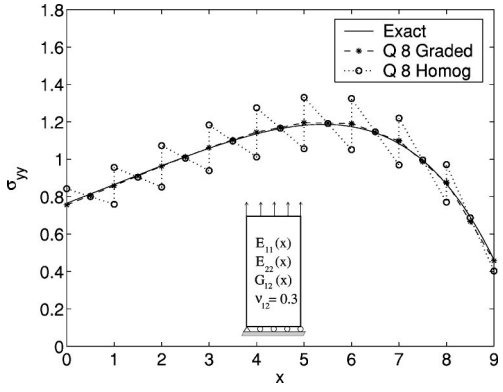

Fig. 22 Stress distribution (σ_{yy}) using Q8 elements for *tension* loading applied perpendicular to the *exponential* material gradation in orthotropic FGMs ($E_{11}^0=1$, $E_{22}^0=0.1$, $G_{12}^0=0.5$, $\nu_{12}=0.3$)

$$E_{11}=[1,2.828], \quad E_{22}=[0.1,0.8], \quad G_{12}=[0.5,1.0].$$

For all other loading cases (i.e., tension and bending perpendicular to the material gradation, and tension parallel to the material gradation), the β_{ij} parameters, characteristic of exponential material variation, are chosen so that the variations of E_{11}, E_{22}, and G_{12} are proportional ([16,17]), i.e.,

$$\beta_{11}=\beta_{22}=\beta_{12}=(\ln 8)/9=\beta, \tag{47}$$

and the γ_{ij} parameters, characteristic of linear material variation, are given by

$$\gamma_{11}=7/9=\gamma, \quad \gamma_{22}=0.7/9, \quad \gamma_{12}=3.5/9$$

so that the range of properties is the following:

$$E_{11}=[1.0,8.0], \quad E_{22}=[0.1,0.8], \quad G_{12}=[0.5,4.0].$$

Regarding the element behavior (homogeneous versus graded), several of the observations made for isotropic materials in the previous section also hold for orthotropic materials. Thus rather than repeating those common observations, this section focuses on new observations and insights. Moreover, the analytical solutions of Section 2 show that, for exponential material gradation (Section 2.1), the relevant stress quantity only depends on the nonhomogeneous parameter β_{22}, and the displacements depend on both β_{11} and β_{22}. For linear material gradation (Section 2.2), the relevant stress depends on γ_{22}, and the displacements depend on both γ_{11} and γ_{22}. This information will be helpful to understand the examples reported below.

For proportional variation of material properties (see Eq. (47)), the change of u_x with x is linear (rather than the nonlinear function of Eq. (9)), which is similar to the behavior of the isotropic plate under the same boundary conditions, i.e., fixed grip (see Fig. 8). This behavior can be seen by the following limit:

$$\lim_{(\beta_{22}-\beta_{11})\to 0} u_x = \lim_{(\beta_{22}-\beta_{11})\to 0} \left\{ -\nu_{12}\varepsilon_0 \frac{E_{22}^0}{E_{11}^0} \frac{1}{\beta_{22}-\beta_{11}} \times [e^{(\beta_{22}-\beta_{11})}-1] \right\}$$

$$= -\nu_{12}\varepsilon_0 \frac{E_{22}^0}{E_{11}^0} x. \tag{48}$$

Figures 21 and 22 compare nodal stresses interpolated from stresses at Gauss points using graded and homogeneous Q4 and Q8 elements, respectively, which are subjected to tension load applied perpendicular to the exponential material gradation. Figure 23 shows a comparison of the displacements (u_x and u_y) computed numerically with those obtained by means of Eq. (18) for all the element types investigated in the present loading case. The curves for u_y indicate that the best elements in terms of matching the analytical solution (Eq. (18)) are Q8 graded, Q8 homogeneous, Q4 graded and Q4 homogeneous, which is somehow expected. Qualitatively, the nodal stress plots considering linear material variation are somewhat similar to those of Figs. 21 and 22 and are not given here ([36]).

A similar comparison is also made for a different loading case consisting of bending applied perpendicular to the material gradation. Figure 24 shows a comparison of the displacements (u_x and u_y) computed numerically with those obtained by Eq. (18) for all the element types investigated in the present loading case. As expected, the Q8 elements capture the analytical solution (Eq. (18)) for u_y better than the Q4 elements. For the sake of brevity, the nodal stress plots are not given here ([36]).

Finally, a few comments regarding the case of tension loading applied parallel to the material gradation in orthotropic FGMs (Fig. 20(*d*)) are in order. Qualitatively, the counterintuitive behavior of homogeneous versus graded Q4 elements is similar to the case involving isotropic nonhomogeneous materials illustrated by Figs. 17 and 18. Thus, for orthotropic case, the Q4 graded element also shows poor performance when compared to the Q4 homogeneous elements for both material variations (i.e., exponential or linear). The reasons for such behavior are given in the last two

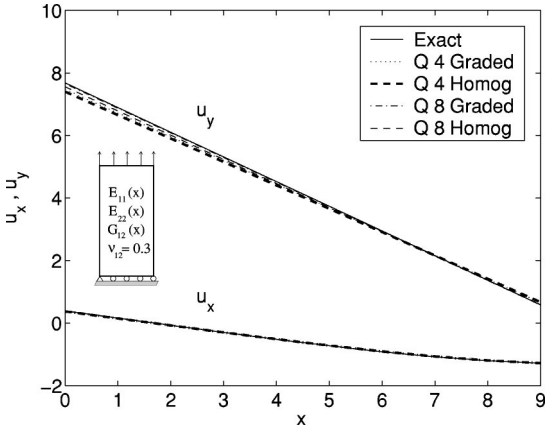

Fig. 23 Displacements (u_x and u_y) along $y=1$ using Q4 and Q8 elements for *tension* load applied perpendicular to the *exponential* material gradation in orthotropic FGMs ($E_{11}^0=1$, $E_{22}^0=0.1$, $G_{12}^0=0.5$, $\nu_{12}=0.3$)

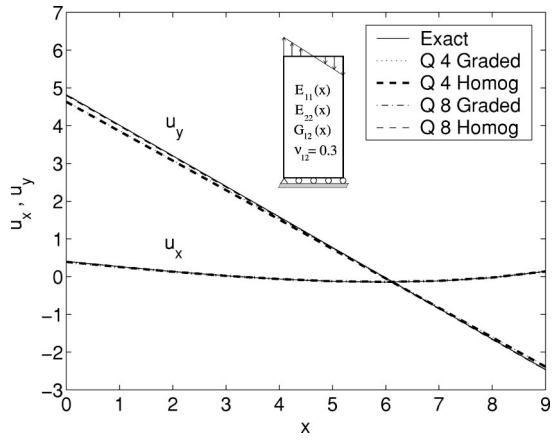

Fig. 24 Displacements (u_x and u_y) along $y=1$ using Q4 and Q8 elements for *bending* load applied perpendicular to the *exponential* material gradation in orthotropic FGMs ($E_{11}^0=1$, $E_{22}^0=0.1$, $G_{12}^0=0.5$, $\nu_{12}=0.3$)

paragraphs of the previous section and will not be repeated here. This is the reverse of the effect seen in the previous load cases for graded orthotropic materials where the graded elements show superior behavior to the corresponding homogeneous elements. Similarly to the isotropic case, a higher-order element such as Q8 (either graded or homogeneous) with 2×2 Gauss quadrature is able to capture the exact solution for this loading case.

5.3 Discussion. This study leads to the following remarks. The isotropic FGM plate (see Fig. 6) has length over width ratio equal to 1 and the orthotropic FGM plate (see Fig. 20) has ratio 2 (for tension and bending loading cases). Because the analytical solution (Section 2) was derived for an infinitely long plate, the higher the aspect ratio (within limits) the better the numerical solution (with respect to the analytical one). For some load cases, e.g., tension and bending perpendicular to the material gradation, the *homogeneous elements* give σ_{yy} as a decreasing function of x in each individual element on the left side of the domain, while the exact solution shows an increasing trend of σ_{yy} with x for this portion of the domain. However, the *graded elements* show the same trend as the exact solution in each element (see, for example, Figs. 11 and 12). The stress plots show that the graded Q8 element gives a smoother stress profile than the graded Q4 element (cf. Figs. 9 and 10). For each loading case, the numerical values of the stress components other than the relevant normal stress quantity should approach zero. Thus the remainder of this paragraph focus on the maximum magnitude of these stress values (obtained numerically) which are theoretically zero. In general, these stress magnitudes are lower with Q8 than with Q4 elements. For tension parallel to the material gradation, the numerical values of the stress σ_{xy} and σ_{yy} are exactly zero for all cases investigated. For the fixed grip case, the largest magnitude of σ_{xy} is $O(10^{-2})$ and occurs for the orthotropic plate with Q4 elements. The largest magnitude of σ_{xx} and σ_{xy} is $O(10^{-3})$ or less for all other analyses for this loading case. For tension and bending perpendicular to the exponential material gradation, the Q4 element leads to spurious shear stresses of $O(10^{0})$ for the orthotropic plate and of $O(10^{-1})$ for the isotropic plate. Smaller magnitudes for the maximum shear stresses are obtained considering linear material gradation. The stress σ_{xx} is of $O(10^{-2})$ or less for all the analyses involving these two loading cases.

6 Concluding Remarks

Graded finite elements, which incorporate the material property gradient at the size scale of the element, have been presented using a *generalized isoparametric formulation*. Both linear (Q4) and quadratic (Q8) quadrilateral elements have been investigated in detail. To address the influence of material property variation, both exponentially and linearly graded elements have been considered and compared. Several plates with continuously nonhomogeneous isotropic and orthotropic materials were considered under fixed grip, tension, and bending conditions. The performance of graded elements was compared to that of conventional elements with respect to analytical solutions.

Higher-order graded elements (e.g., quadratic and higher) are superior to conventional homogeneous elements based on the same shape functions. One should be careful when using graded elements with linear shape functions (e.g., Q4) as it may lose accuracy in certain situations such as uniform traction parallel to the material gradient direction. When using this element, we recommend to average the nodal properties of the element, which would convert it to a regular homogeneous element. Thus the value of material properties at the integration points used to compute stresses depend on whether first-order or higher-order elements are used. This simple procedure leads to a more robust element. A similar procedure is used in the finite element code ABAQUS ([37]) for heat transfer analysis and also in the WARP3D code ([38]).

Acknowledgments

We gratefully acknowledge the support from the National Science Foundation (NSF) under grant No. CMS-0115954 (Mechanics and Materials Program) and from the NASA Ames Research Center (NAG 2-1424) to the University of Illinois at Urbana-Champaign.

References

[1] Hirai, T., 1996, "Functionally Graded Materials," *Materials Science and Technology: Processing of Ceramics, Part 2*, R. J. Brook, ed., VCH Verlagsgesellschaft mbH, Weinheim, Germany, **17B**, pp. 292–341.
[2] Miyamoto, Y., Kaysser, W. A., Rabin, B. H., Kawasaki, A., and Ford, R. G., 1999, *Functionally Graded Materials: Design, Processing, and Applications*, Kluwer, MA.
[3] Suresh, S., and Mortensen, A., 1998, *Fundamentals of Functionally Graded Materials*, IOM Communications, London.
[4] Koizumi, M., 1993, "The concept of FGM," *Proceedings of the Second International Symposium on Functionally Gradient Materials, Ceramic Transactions*, J. B. Holt et al., eds., Westerville, Ohio, The American Ceramic Society, **34**, pp. 3–10.
[5] Pindera, M.-J., Aboudi, J., and Arnold, S. M., 1998, "Thermomechanical Analysis of Functionally Graded Thermal Barrier Coatings With Different Microstructural Scales," J. Am. Ceram. Soc., **81**(6), pp. 1525–1536.
[6] Tokita, M., 1999, "Development of Large-Size Ceramic/Metal Bulk FGM Fabricated by Spark Plasma Sintering," Mater. Sci. Forum, **308–311**, pp. 83–88.
[7] Sampath, S., Hermann, H., Shimoda, N., and Saito, T., 1995, "Thermal Spray Processing of FGMs," M.R.S. Bull., **20**(1), pp. 27–31.
[8] Kaysser, W. A., and Ilschner, B., 1995, "FGM Research Activities in Europe," M.R.S. Bull., **20**(1), pp. 22–26.
[9] Markworth, A. J., Ramesh, K. S., and Parks, Jr., W. P., 1995, "Modelling Studies Applied to Functionally Graded Materials," J. Mater. Sci., **30**, pp. 2183–2193.
[10] Lee, Y. D., and Erdogan, F., 1995, "Residual/Thermal Stresses in FGM and Laminated Thermal Barrier Coatings," Int. J. Fract., **69**, pp. 145–165.
[11] Kurihara, K., Sasaki, K., and Kawarada, M., 1990, "Adhesion Improvement of Diamond Films," *Proceedings of the First International Symposium on Functionally Gradient Materials*, M. Yamanouchi et al., eds., Tokyo, Japan.
[12] Jin, Z.-H., and Paulino, G.H., 2001, "Transient Thermal Stress Analysis of an Edge Crack in a Functionally Graded Material," Int. J. Fract., **107**(1), pp. 73–98.
[13] Hasselman, D. P. H., and Youngblood, G. E., 1978, "Enhanced Thermal Stress Resistance of Structural Ceramics With Thermal Conductivity Gradient," J. Am. Ceram. Soc., **61**(1–2), pp. 49–52.
[14] Horgan, C. O., and Chan, A. M., 1999, "Pressurized Hollow Cylinder or Disk Problem for Functionally Graded Isotropic Linearly Elastic Materials," J. Elast., **55**(1), pp. 43–59.
[15] Carpenter, R. D., Liang, W. W., Paulino, G. H., Gibeling, J. C., and Munir, Z. A., 1999, "Fracture Testing and Analysis of a Layered Functionally Graded Ti/TiB Beam in 3-Point Bending," Mater. Sci. Forum, **308–311**, pp. 837–842.
[16] Ozturk, M., and Erdogan, F., 1997, "Mode I Crack Problem in an Inhomogeneous Orthotropic Medium," Int. J. Eng. Sci., **35**(9), pp. 869–883.
[17] Ozturk, M., and Erdogan, F., 1999, "The Mixed Mode Crack Problem in an Inhomogeneous Orthotropic Medium," Int. J. Fract., **98**, pp. 243–261.
[18] Paulino, G. H., and Jin, Z.-H., 2000, "Viscoelastic Functionally Graded Ma-

terials Subjected to Antiplane Shear Fracture,'' ASME J. Appl. Mech., **68**(1), pp. 284–293.
[19] Aboudi, J., Pindera, M.-J., and Arnold, S. M., 1999, ''Higher-Order Theory for Functionally Graded Materials,'' Composites, Part B, **30**, pp. 777–832.
[20] Pindera, M.-J., and Dunn, P., 1997, ''Evaluation of the Higher-Order Theory for Functionally Graded Materials Via the Finite-Element Method,'' Composites, Part B, **28**(1/2), pp. 109–119.
[21] Goldberg, R. K., and Hopkins, D. A., 1995, ''Thermal Analysis of a Functionally Graded Material Subject to a Thermal Gradient Using the Boundary Element Method,'' Compos. Methods Appl. Mech. Eng., **5**(7), pp. 793–806.
[22] Sutradhar, S., Paulino, G. H., and Gray, L. J., 2002, ''Transient Heat Conduction in Homogeneous and Non-Homogeneous Materials by the Laplace Transform Galerkin Boundary Element Method,'' Eng. Anal. Bound. Elem., **26**(2), pp. 119–132.
[23] Eischen, J. W., 1987, ''Fracture of Nonhomogeneous Materials,'' Int. J. Fract., **34**, pp. 3–22.
[24] Williamson, R. L., Rabin, B. H., and Drake, J. T., 1993, ''Finite Element Analysis of Thermal Residual Stresses at Graded Ceramic-Metal Interfaces, Part I: Model Description and Geometric Effects,'' J. Appl. Phys., **74**(2), pp. 1310–1320.
[25] Drake, J. T., Williamson, R. L., and Rabin, B. H., 1993, ''Finite Element Analysis of Thermal Residual Stresses at Graded Ceramic-Metal Interfaces, Part II: Interface Optimization for Residual Stress Reduction,'' J. Appl. Phys., **74**(2), pp. 1321–1326.
[26] Giannakopoulos, A. E., Suresh, S., Finot, M., and Olsson, M., 1995, ''Elastoplastic Analysis of Thermal Cycling: Layered Materials With Compositional Gradients,'' Acta Mater., **43**(4), pp. 1335–1354.
[27] Gu, P., Dao, M., and Asaro, R. J., 1999, ''A Simplified Method for Calculating the Crack-Tip Field of Functionally Graded Materials Using the Domain Integral,'' ASME J. Appl. Mech., **66**(1), pp. 101–108.
[28] Dao, M., Gu, P., Maewal, A., and Asaro, R. J., 1997, ''A Micromechanical Study of Residual Stresses in Functionally Graded Materials,'' Acta Mater., **45**(8), pp. 3265–3276.
[29] Anlas, G., Santare, M. H., and Lambros, J., 2000, ''Numerical Calculation of Stress Intensity Factors in Functionally Graded Materials,'' Int. J. Fract., **104**, pp. 131–143.
[30] Santare, M. H., and Lambros, J., 2000, ''Use of Graded Finite Elements to Model the Behavior of Nonhomogeneous Materials,'' ASME J. Appl. Mech., **67**, pp. 819–822.
[31] Kim, J.-H., and Paulino, G. H., 2002, ''Finite Element Evaluation of Mixed Mode Stress Intensity Factors in Functionally Graded Materials,'' Int. J. Numer. Methods Eng., **53**(8), pp. 1903–1935.
[32] Erdogan, F., and Wu, B. H., 1997, ''The Surface Crack Problem for a Plate with Functionally Graded Properties,'' ASME J. Appl. Mech., **64**, pp. 449–456.
[33] Paulino, G. H., and Kim, J.-H., ''The Weak Patch Test for Nonhomogeneous Materials Modeled With Graded Finite Elements'' (submitted for publication).
[34] Hughes, T. J. R., 1987, *The Finite Element Method: Linear Static and Dynamic Finite Element Analysis*, Prentice-Hall, Englewood Cliffs, NJ.
[35] Jin, Z.-H., Paulino, G. H., and Dodds, Jr., R. H., 2002, ''Finite Element Evaluation of Quasi-Static Crack Growth in Functionally Graded Materials Using a Novel Cohesive Zone Fracture Model,'' ASME J. Appl. Mech., **69**, pp. 370-379.
[36] Kim, J.-H., ''Quasi-Static Crack Propagation in Functionally Graded Materials,'' Ph.D. thesis, University of Illinois at Urbana-Champaign, Urbana, IL.
[37] Hibbitt, Karlson, & Sorensen, Inc., 2000, *ABAQUS/Standard User's Manual*, Vol. II, Pawtucket, RI, Version 6.1 (p. 14.1.1-14).
[38] Gullerud, A. S., Koppenhoefer, K. C., Roy, A., Roychowdhury, S., and Dodds, Jr., R. H., 2001, *WARP3D-Release 13.11*, University of Illinois, UILU-ENG-95-2012.